Colloids and Surfaces B: Biointerfaces 110 (2013) 8–14

Contents lists available at SciVerse ScienceDirect

Colloids and Surfaces B: Biointerfaces

journal homepage: www.elsevier.com/locate/colsurfb

Graphene and CdS nanocomposite: A facile interface for construction of DNA-based electrochemical biosensor and its application to the determination of phenformin

Lijiao Zeng, Rui Wang, Lihua Zhu, Jingdong Zhang*

School of Chemistry and Chemical Engineering, Huazhong University of Science and Technology, Luoyu Road 1037, Wuhan 430074, PR China

ARTICLE INFO

Article history:
Received 7 December 2012
Received in revised form 22 March 2013
Accepted 22 April 2013
Available online 28 April 2013

Keywords:
Graphene/CdS
Nanocomposite
DNA
Electrochemical biosensor
Phenformin

ABSTRACT

Graphene/cadmium sulphide (GR-CdS) nanocomposite was synthesized via a low temperature process in aqueous solution. The as-prepared nanocomposite was characterized by scanning electron microscopy, UV–visible spectroscopy, Fourier transform infrared spectroscopy, and X-ray diffraction. The impedance analysis indicated that GR-CdS nanocomposite possessed outstanding electrochemical performance for facile electron transfer. When DNA was immobilized on GR-CdS (DNA/GR-CdS) modified electrode, the electrochemical oxidation of guanine and adenine in DNA residue bases was significantly promoted. Due to the interaction of DNA with phenformin, the voltammetric current of guanine or adenine on the DNA/GR-CdS electrode was decreased when phenformin was present in the electrolytic solution. Under optimized conditions, the signal of guanine on DNA/GR-CdS electrode decreased linearly with increasing the concentration of phenformin in the range of 1.0×10^{-6} mol L^{-1} to 1.0×10^{-3} mol L^{-1}. The proposed DNA-based electrochemical biosensor was successfully applied to the determination of phenformin in real samples.

1. Introduction

The electroactive purine bases in DNA molecule have endowed this genetic material with useful electrochemical features. Based on the change of electrochemical signals generated on DNA bases, various electrochemical DNA biosensors have been constructed for studying DNA hybridization [1–3], DNA damage [4–6], DNA interaction with small molecules [7–9], and monitoring organic compounds [10–13]. However, DNA bases usually exhibit very weak electrochemical signals on conventional electrodes. To overcome this problem, various nanomaterials such as metal nanoparticles [14], carbon nanotubes [15], graphene [16,17] and TiO_2 [18], and nanocomposites such as cobalt phthalocyanine–carbon nanotube complexes [19] have been utilized to modify the electrodes, which could promote the electrochemical response of DNA and improve the sensitivity of DNA-based biosensors.

Recently, the nanocomposites of CdS and graphene (GR) have attracted considerable interest in various fields due to their unique physicochemical properties and synergetic effects of nanomaterials. Cao et al. have reported a facile one-step method to prepare GR-CdS nanocomposites with good optoelectronic properties [20]. Li et al. have developed a hydrothermal method to prepare CdS cluster-decorated graphene nanosheets for highly efficient visible-light-driven photocatalytic hydrogen production [21]. In electrochemistry, GR-CdS nanocomposites have shown to be useful electrode materials for the preparation of sensors. Based on GR-CdS nanocomposites, a sensitive electrochemical immunosensor for cancer biomarker determination [22] and electrochemiluminescence sensing of H_2O_2 [23] have been demonstrated.

Phenformin (Fig. 1) is a biguanide antidiabetic agent that can modulate glucose metabolism and promote weight loss. This pharmaceutical drug has been used for the management of type II diabetes. Moreover, phenformin has been found to possess novel features, such as suppression of calcium responses to glutamate and protection of hippocampal neurons against excitotoxicity [24], antitumor activity [25], inhibitory effect on the ATP-sensitive potassium channel [26] and blockage of the peripheral antinociception induced by diclofenac [27]. Therefore, determining phenformin in pharmaceutical drugs and biological fluids is of particular importance. Various instrumental methods such as capillary electrophoresis [28], HPLC [29], spectrophotometry [30], and chemiluminescence [31] have been established to determine phenformin.

In the present work, we developed a new method for the synthesis of GR-CdS nanocomposite in aqueous solution which did not require high temperature, high pressure, or toxic organic reagents usually adopted in previously reported methods. When GR-CdS nanocomposite was utilized to modify glassy carbon electrode, the

* Corresponding author. Tel.: +86 27 87792154; fax: +86 27 87543632.
E-mail address: zhangjd@mail.hust.edu.cn (J. Zhang).

0927-7765/$ – see front matter © 2013 Elsevier B.V. All rights reserved.
http://dx.doi.org/10.1016/j.colsurfb.2013.04.025

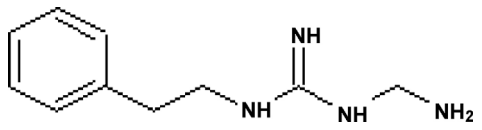

Fig. 1. Structure of phenformin.

voltammetric response of DNA was remarkably improved. Based on such a DNA/GR-CdS electrode, a novel DNA-based electrochemical biosensor for determining phenformin was demonstrated. Compared with other instrumental methods, this biosensor could offer the advantages of electrochemical technique such as simple instrumentation, fast response and low cost. Moreover, the biosensor could overcome the difficulty in the direct electrochemical detection of phenformin which showed a weak voltammetric response on solid electrodes.

2. Experimental

2.1. Chemicals

Phenformin hydrochloride standard sample (≥99.0%) was provided by Wuhan Yuancheng Gongchuang Technology Co., Ltd. (Wuhan, China). Phenformin tablet was purchased from Shandong Renhetang Pharmaceutical Co., Ltd. (Shandong, China). Herring sperm DNA was obtained from Sigma. Chitosan (CHIT) (degree of deacetylation >90.0%) was provided by Shanghai Ruji Biological Technology Co., Ltd. (Shanghai, China). Other chemicals were of analytical grade. Doubly distilled water was used throughout the investigation.

2.2. Synthesis of GR-CdS nanocomposite

Graphene oxide (GO) was prepared from graphite powder according to a modified Hummers method as described previously [32]. To prepare GR-CdS nanocomposite, GO (50 mg) and $CdCl_2{\cdot}2.5H_2O$ (228 mg) were dissolved in 100 mL water, with adding 1 mL mercaptoacetic acid to prevent aggregation of CdS nanoparticles. The solution pH was adjusted to 9.0 with 1.0 mol L^{-1} NaOH, and then transferred to a 250-mL three-necked flask and reacted under 90 °C in a thermostatic bath with nitrogen agitation. After 30 min, $Na_2S{\cdot}9H_2O$ (120 mg) was added and the reaction was continued for another 5 h. The black precipitate was collected, harvested by centrifugation and dried in oven at 60 °C for 24 h. As a control, free GR and CdS nanoparticles were also synthesized under the same reaction conditions without the addition of $CdCl_2$ or GO, respectively.

2.3. Electrode modification and DNA immobilization

Prior to modification, the surface of glass carbon electrode (GCE) was polished to a mirror-like smoothness with emery papers, and then washed successively with ethanol and water. After dried with nitrogen gas, the GCE surface was coated with 5 μL of 1 mg mL^{-1} GR-CdS suspension, which was prepared by dispersing GR-CdS in 0.035% CHIT aqueous solution containing 0.52% acetic acid with the aid of 5 h ultrasonic agitation. Since GR-CdS was difficult to be dispersed in pure water, CHIT was used as dispersant to obtain a homogenous and stable suspension of GR-CdS. Moreover, the high positive charge density of CHIT was helpful to improve the immobilization of DNA owing to the electrostatic interaction between CHIT and DNA [33].

The immobilization of DNA on the surface of GR-CdS/GCE was carried out by immersing the electrode in 0.7 mg mL^{-1} DNA dissolved in 0.2 mol L^{-1} phosphate buffer solution (PBS) (pH 7.0), followed by applying +0.5 V bias potential for 200 s. The applied positive bias potential allowed the adsorption of negatively charged DNA on the GR-CdS/GCE surface. Before electrochemical measurements, the electrodes were rinsed thoroughly with deionized water to remove the loosely adsorbed DNA.

2.4. Apparatus and procedure

Scanning electron microscopic (SEM) images were obtained with a Quanta 200 field emission scanning electron microscope (FEI, Netherlands). X-ray diffraction (XRD) measurements were carried out on a Philips X'pert Pro X-ray diffractometer (PANalytical, Netherlands) equipped with a Cu Kα radiation source (λ = 1.5406 Å). The accelerating voltage and applied current were 40 kV and 40 mA, respectively. Fourier transform infrared (FTIR) spectra were recorded on an Equinox 55 FTIR spectrometer (Bruker, Germany). UV–visible spectra were measured with a TU-1900 UV/Vis spectrophotometer (Beijing Purkinje General Instrument Company, China).

Voltammetric experiments were performed on an EC550 electrochemical workstation (Wuhan Gaoss Union Instrument Company, China) and electrochemical impedance spectra (EIS) were recorded with a CHI660A electrochemical workstation (Shanghai Chenghua Instrument Company, China). All electrochemical measurements were carried out in a conventional three-electrode system, which consisted of a bare or modified GCE (2.5 mm in diameter) working electrode, a platinum wire auxiliary electrode and a saturated calomel reference electrode (SCE). For differential pulse voltammetry (DPV), the parameters were: pulse height: 50 mV, pulse width: 50 mV, pulse period: 0.2 s. For EIS, the parameters were: frequency: 0.01 Hz to 100 kHz, applied potential: +0.20 V, amplitude: 5 mV.

The high performance liquid chromatography (HPLC) analysis was performed on an Agilent 1100 HPLC system (Agilent, USA) with a C18 column. An aliquot of 20 μL sample was injected into the HPLC system. The mobile phase consisted of hydrogen ammonium phosphate buffer (pH 3.5) and methanol (75:25, v/v), and the flow rate was 1.0 mL min^{-1}. The detection was carried out at 235 nm using a diode-array detector.

3. Results and discussion

3.1. Characterization of synthesized GR-CdS

The morphology of synthesized products namely GO, GR, CdS and GR-CdS was characterized with SEM (Fig. 2). From Fig. 2a, the feature of GO represented by a sheet-like structure with some slight wrinkles could be observed. While GO was transferred to GR after 5-h thermal reduction reaction, GO sheet was fragmented to a folding block structure (Fig. 2b). For synthesized CdS, many nanoparticles in the diameter of ca. 20 nm were found although some CdS nanoparticles were aggregated to form bigger nanoparticles in the diameter of ca. 60–70 nm (Fig. 2c). For GR-CdS, it was clear that many CdS nanoparticles were embedded into the GR sheets (Fig. 2d).

Fig. 3A illustrates the XRD patterns of synthesized products. The XRD pattern of GO showed a sharp peak at 9.06° (curve a in Fig. 3A), corresponding to the reflection angle of GO [34]. After the thermal reduction of GO, the feature diffraction peak at 9.06° disappeared and a broad diffraction peak with low intensity centered at 25.5° corresponding to graphene [35] was observed (curve b in Fig. 3A). The diffraction peaks of CdS (curve c in Fig. 3A) appeared at 26.0°, 43.6° and 51.4° corresponding respectively to (1 1 1), (2 2 0) and (3 1 1) crystal planes of CdS [20], which matched well with those of cadmium yellow CdS phase (JCPDS 41-1049). For GR-CdS

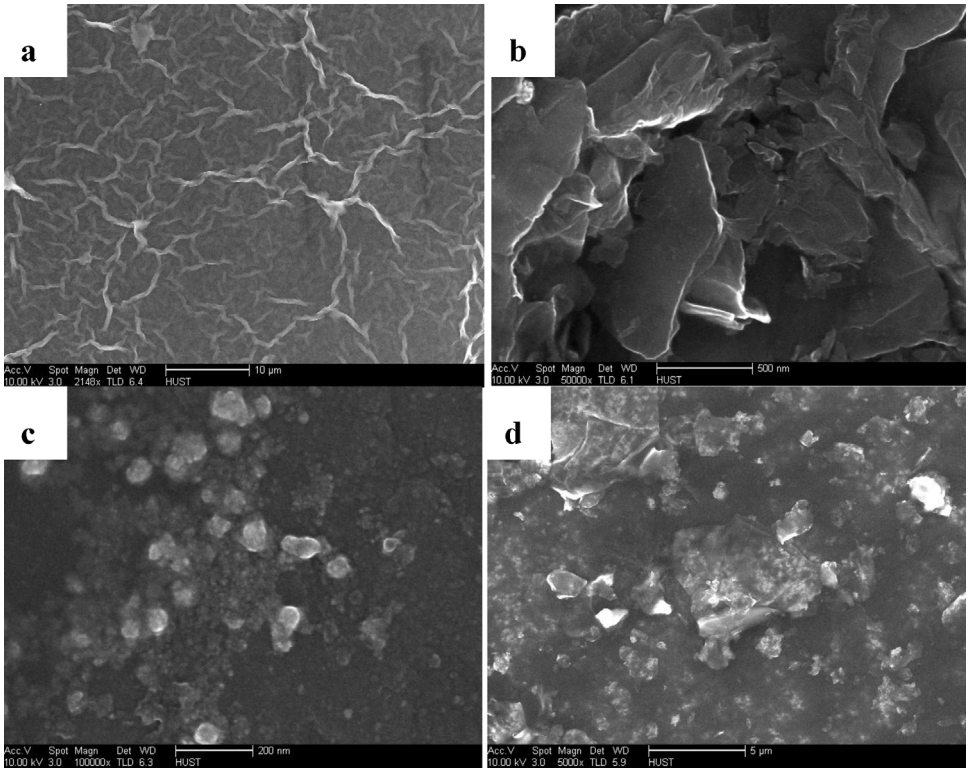

Fig. 2. SEM images of (a) GO, (b) GR, (c) CdS, and (d) GR-CdS nanocomposite.

composite, the XRD pattern (curve d in Fig. 3A) only showed the diffraction peaks of CdS crystals but without the peak of GO, confirming the formation of CdS on reduced GO by the proposed preparation method.

Fig. 3B compares the UV–visible absorption spectra of GO, GR, CdS and GR-CdS. It could be seen that GO showed a relatively strong absorption peak at 227 nm (curve a in Fig. 3B), attributed to the π–π^* transition of oxygen-containing groups of GO. While GO was transferred to GR, the oxygen-containing groups was reduced. Thus, the UV–visible absorption spectrum of GR had no absorption peak (curve b in Fig. 3B). In the case of GR-CdS nanocomposite (curve d in Fig. 3B), the absorption in the wavelength range from 200 nm to 450 nm was obviously higher than GR, owing to the strong absorption of CdS exhibiting up to 450 nm (curve c in Fig. 3B) resulted from the optical excitation of electrons across the band gap of semiconductor [36].

The FTIR spectrum of GO (curve a in Fig. 3C) showed three absorption bands at 1731 cm^{-1}, 1400 cm^{-1} and 1052 cm^{-1}, corresponding to the C=O stretching of COOH groups situated at edges of the GO sheets, tertiary C—OH groups stretching and C—O stretching vibrations of aromatic nucleus, respectively [20]. The band at 1622 cm^{-1} was assigned to the skeletal vibration of the unoxidized graphite domains [37]. While in the FTIR spectra of GR and GR-CdS, almost all of the bands related to oxygen-containing groups of GO were removed or shifted (curves b and d in Fig. 3C), confirming the reduction of these oxygen-containing groups [38]. Moreover, two absorption bands appeared at ca. 1580 cm^{-1} and 1390 cm^{-1} for GR, CdS and GR-CdS were ascribed to the antisymmetric and symmetric carboxylate stretch absorptions generated from mercaptoacetic acid [39] used in the synthesis process.

3.2. Electrochemical impedance analysis

To characterize the electrochemical performance of GR-CdS, the GR-CdS modified GCE was studied by EIS using $[Fe(CN)_6]^{3-/4-}$ redox probe and compared with other electrodes. Fig. 4 shows the Nyquist plots of various electrodes and the corresponding equivalent circuits. The EIS data were analyzed by fitting them to the corresponding equivalent circuit models using Zview software. The result showed that the electron transfer resistance (R_p) for bare GCE (curve a in Fig. 4A) was 4.87 kΩ. When GCE was modified with GO (Fig. 4B), the R_p value was dramatically increased to 26.08 kΩ, due to the prohibition of the negative charged GO to the electron transfer of $[Fe(CN)_6]^{3-/4-}$. While GCE was modified with CdS (curve b in Fig. 4A), the R_p value was decreased to 2.99 kΩ, indicating the promotion of CdS to the electron transfer of $[Fe(CN)_6]^{3-/4-}$. For GR/GCE (curve a in Fig. 4C), the Nyquist plot displayed a straight line while the semicircle observed on GCE disappeared, representing the typical characteristic of a diffusion limiting step [40,41]. This result is quite different from that of GO, due to the increased conductivity of GR nanosheet when the oxygen-containing group of GO is decomposed to oxygen-free GR [42]. For GR-CdS/GCE (curve b in Fig. 4C), the Nyquist plot also displayed a straight line. However, the straight line of Nyquist plot for GR-CdS/GCE was steeper than that for GR/GCE, demonstrating the superior electron transfer performance of GR-CdS composite. On the other hand, when DNA was immobilized on GR-CdS/GCE by electro-adsorption, a semi-circle corresponding to the R_p value of 1.55 kΩ was observed in the Nyquist plot (curve c in Fig. 4A), demonstrating the effective immobilization of negatively charged DNA on GR-CdS/GCE surface which prohibited the electron transfer of $[Fe(CN)_6]^{3-/4-}$.

3.3. Electrochemical behavior of DNA immobilized on GR-CdS modified electrode

3.3.1. Comparison of voltammetric responses of DNA immobilized on different electrodes

DNA is well-known to have electroactive purine bases (guanine and adenine) and pyrimidine bases (cytosine and thymine).

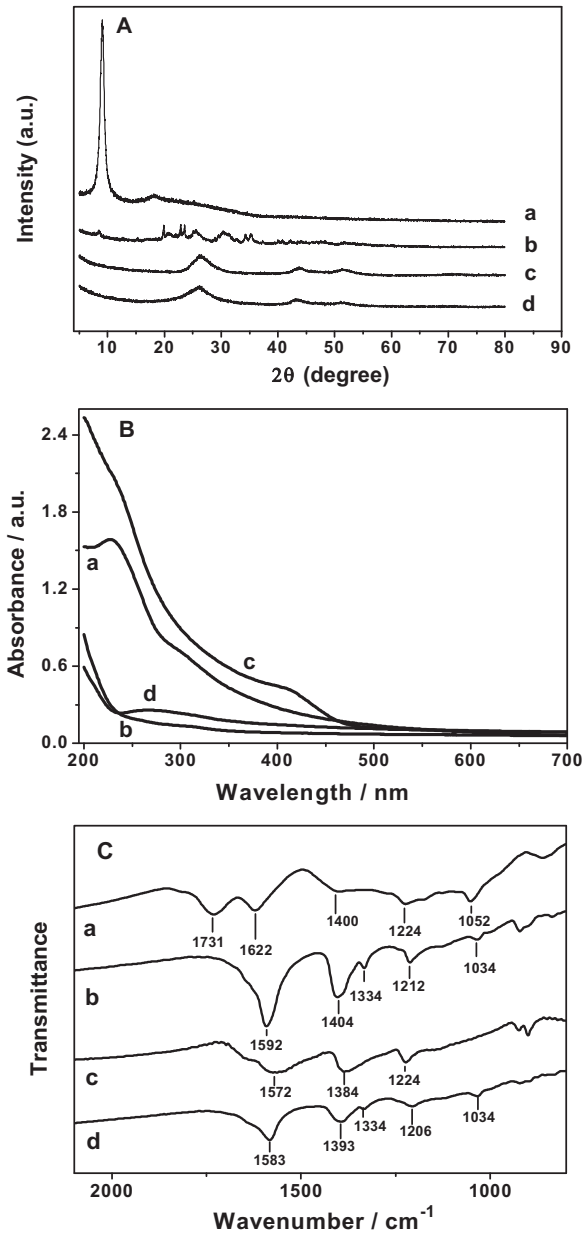

Fig. 3. (A) XRD patterns, (B) UV–vis spectra, and (C) FTIR spectra of (a) GO, (b) GR, (c) CdS, and (d) GR-CdS.

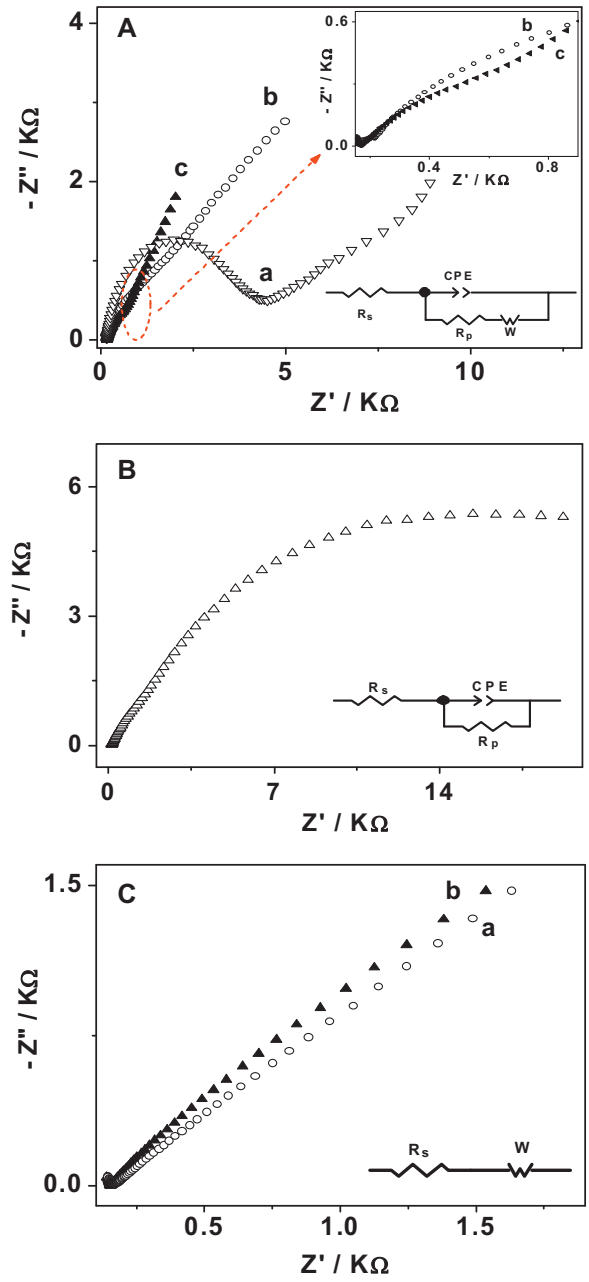

Fig. 4. Nyquist plots for $K_3[Fe(CN)_6]/K_4[Fe(CN)_6]$ (10 mmol L^{-1}, 1:1) in 0.1 mol L^{-1} KCl at (A) (a) GCE, (b) CdS/GCE, and (c) DNA/GR-CdS/GCE; (B) GO/GCE; and (C) (a) GR/GCE and (b) GR-CdS/GCE. The insets in the lower right corner represent the corresponding equivalent circuits (R_s = solution resistance, R_p = electron transfer resistance, W = Warburg impedance, CPE = constant phase element). The inset in upper right corner of (A) shows the enlarged parts of (b) and (c).

Since purine bases require lower overpotential for oxidation than pyrimidines [43], the oxidation signals of purine bases are easily observed on various DNA-immobilized electrodes. Our experiments confirmed the electrochemical oxidation signals of purine bases in DNA. However, DNA exhibited a very weak electrochemical response after being immobilized on bare GCE (curve a in Fig. 5). Even after GCE was modified with CdS, the electrochemical response of immobilized DNA was not obviously promoted (curve b in Fig. 5). While GCE was modified with GO, GR or GR-CdS, two well-defined oxidation peaks were clearly observed at about 0.7 V and 1.0 V attributed, respectively, to the electrochemical oxidation of guanine and adenine residues, indicating the promotion of these materials to the electron transfer of DNA. Further comparison showed that GR-CdS was the most effective material to enhance the electrochemical response of DNA. It is likely that CdS further promotes the electron transfer between DNA and GR although CdS does not facilitate the direct electron transfer between DNA and GCE. Moreover, CdS increases the surface area of nanocomposite to allow more DNA immobilized on the electrode surface. The amplified signal of DNA on GR-CdS/GCE demonstrates that GR-CdS nanocomposite is promising to construct DNA-based electrochemical biosensors with improved sensitivity.

3.3.2. Influences of pH, adsorption potential, adsorption time and DNA concentration

Fig. 6 shows the influence of pH on the voltammetric response of DNA/GR-CdS/GCE. It was observed that both the peak potentials of guanine and adenine shifted negatively with increasing the pH value of solution from 5.8 to 7.8 (Fig. 6A). A linear relationship existed between the oxidation peak potential of guanine and solution pH (curve a in Fig. 6B), which was expressed as

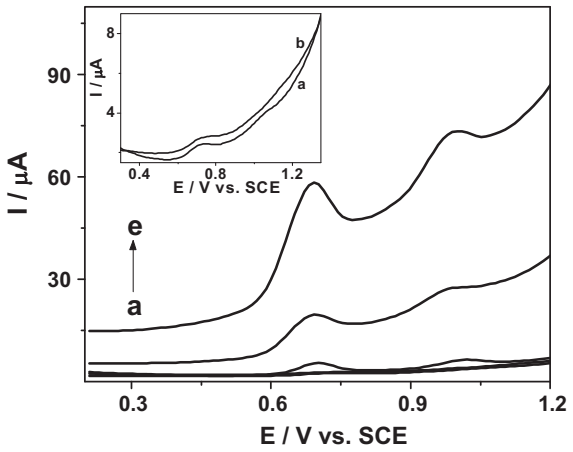

Fig. 5. DPVs of DNA immobilized on (a) bare GCE, (b) CdS/GCE, (c) GO/GCE, (d) GR/GCE, and (e) GR-CdS/GCE. Electrolyte: 0.2 mol L^{-1} PBS (pH 7.0). Adsorption potential: 0.5 V. Adsorption time: 200 s. DNA concentration: 0.5 mg mL^{-1}. Inset: enlarged DPV curves of (a) bare GCE and (b) CdS/GCE.

E_p(V) = 1.27 − 0.0827 pH with a correlation coefficient (r) of 0.998, meaning the participation of proton in the electrochemical process of DNA [44,45]. Moreover, the peak current of guanine (i_p) increased with solution pH up to 7.0 and then declined when solution pH was further increased (curve b in Fig. 6B). This result could be explained by two roles of pH in adsorption and electrochemical processes of DNA. On one hand, the negative charges of phosphate functional groups of DNA molecules are decreased with decreasing the solution pH [46], leading to reduced adsorption amount of DNA

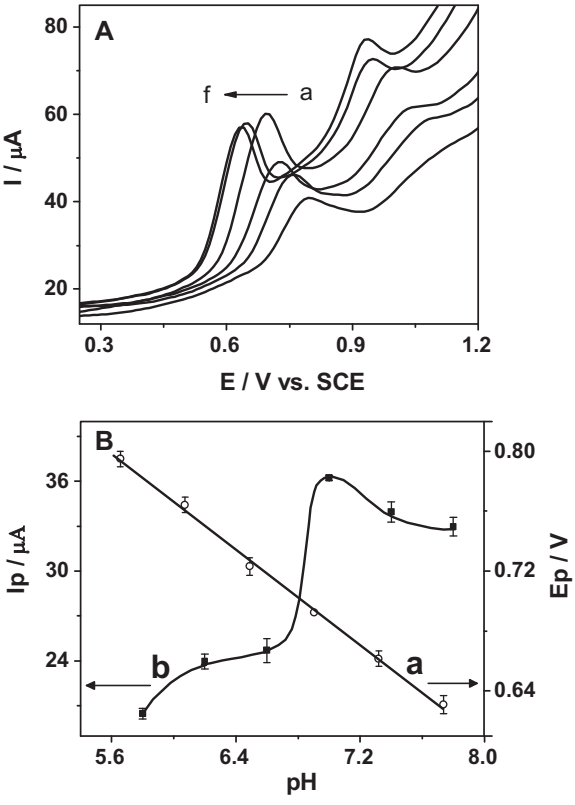

Fig. 6. (A) DPVs of DNA/GR-CdS/GCE at different pH: (a) 5.8, (b) 6.2, (c) 6.6, (d) 7.0, (e) 7.4, and (f) 7.8. (B) Influence of pH on (a) peak potential and (b) peak current of guanine. Adsorption potential: 0.5 V. Adsorption time: 200 s. DNA concentration: 0.5 mg mL^{-1}. Error bars were derived from the standard deviation of four measurements.

on the electrode surface. Thus, the peak current of DNA is reduced by lowering pH value below 7.0. On the other hand, since proton participates the electrochemical process of DNA, the shortage of proton restrains the oxidation of DNA when solution pH is higher than 7.0. Therefore, pH 7.0 was selected as the optimum pH for the sensor.

The immobilization methodology plays an important role in the construction of DNA-based biosensors. Although adsorption is the simplest method to immobilize DNA on surfaces [47], electrochemically assisted adsorption of DNA has been widely adopted to stabilize the DNA on the transducer surface, in which the electrostatic interaction between the positively charged electrode and the negatively charged phosphate backbone increases the stability of the adsorbed DNA [48]. Our study demonstrated that the electrochemical response of DNA immobilized on GR-CdS/GCE was obviously influenced by the adsorption potential. It was seen that the peak current of guanine increased gradually with increasing the adsorption potential from +0.1 V to +0.5 V (Fig. 7A), implying that positive bias potential could improve the amount of DNA immobilized on the electrode surface and enhance the stability of DNA film due to the strong electrostatic attraction between the positively charged electrode and negatively charged DNA. However, when the applied potential exceeded +0.5 V, the faradic current reduced inversely, which might be owing to the oxidation of DNA under too high potential. Moreover, the adsorption time and DNA concentration also showed obvious effects on the electrochemical response of DNA/GR-CdS/GCE (Fig. 7B and C). The electrochemical peak current of guanine was increased when the adsorption time was prolonged from 50 s to 200 s or the concentration of DNA was increased from 0.1 mg mL^{-1} to 0.7 mg mL^{-1}. When the adsorption time was longer than 200 s or the DNA concentration was higher than 0.7 mg mL^{-1}, the adsorption of DNA on the electrode reached the saturated state and the electrochemical response of DNA/GR-CdS/GCE did not show further enhancement. Thus, +0.5 V applied potential, 200 s adsorption time and 0.7 mg mL^{-1} DNA were chosen as the optimum conditions for the construction of DNA-based electrochemical sensor.

3.4. Electrochemical sensing of phenformin on DNA/GR-CdS/GCE

3.4.1. Calibration analysis

The cyclic voltammetric measurements indicated that 1×10^{-3} mol L^{-1} phenformin generated a very weak electrochemical response on either bare GCE or GR-CdS modified GCE. In comparison, DNA/GR-CdS/GCE responded sensitively to 1×10^{-3} mol L^{-1} phenformin. As illustrated in Fig. 8A, the voltammetric peak current of DNA on DNA/GR-CdS/GCE was reduced when phenformin was present in the electrolyte solution, due to the interaction of DNA with phenformin. The variation of peak current was estimated by the percentage of deceased response (R%) [32], which is the ratio of guanine peak current before (I_b) and after (I_a) interaction with phenformin, namely $R\% = (I_b - I_a)/I_b \times 100$. Under optimum conditions mentioned above, a linear relationship was found between R% and the concentration of phenformin from 1.0×10^{-6} mol L^{-1} to 1.0×10^{-3} mol L^{-1}. The linear regression equation was expressed as $R\% = 1.60 + 46.1c$ (mmol L^{-1}) (n = 7, r = 0.996). The limit of detection (LOD) (3S/N) was estimated to be 3.34×10^{-7} mol L^{-1}. Compared with the previously reported results for phenformin determination (Table 1), the LOD of this electrochemical biosensor method was lower than spectrophotometry [30], but a little higher than HPLC [29] and chemiluminescence [31].

To evaluate the reproducibility of the biosensor, the responses of six DNA/GR-CdS/GCE electrodes independently constructed were tested in 1×10^{-4} mol L^{-1} phenformin in PBS (pH 7.0). The relative standard deviation (RSD) was 1.10%, showing good reproducibility

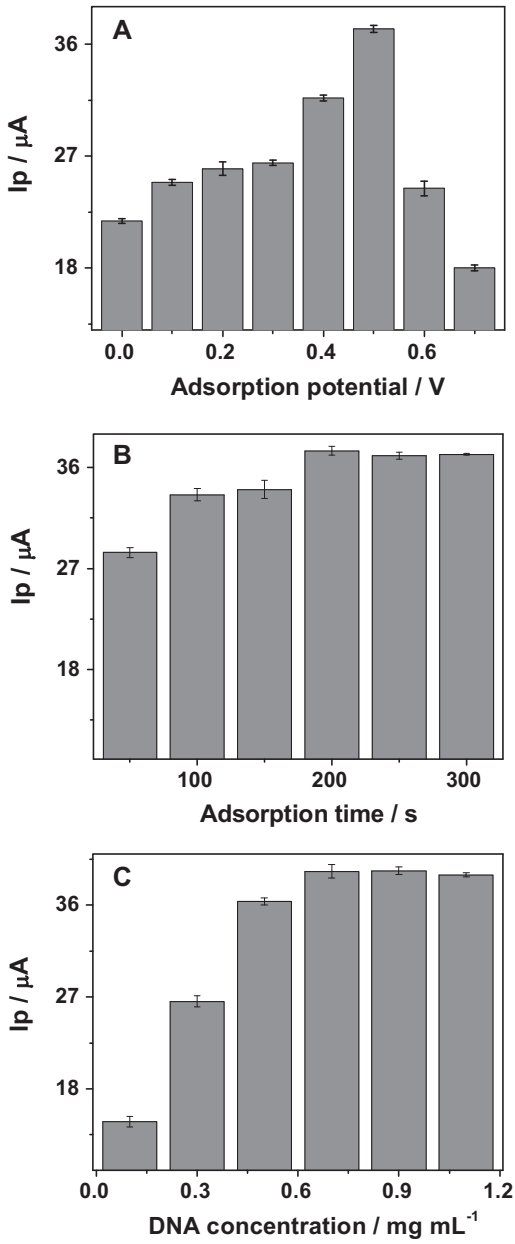

Fig. 7. Influences of (A) adsorption potential, (B) adsorption time, and (C) DNA concentration on the peak current of guanine on DNA/GR-CdS/GCE. Error bars were derived from the standard deviation of four measurements.

and precision of the proposed biosensor. On the other hand, the selectivity of the biosensor was studied by comparing the responses of DNA/GR-CdS/GCE in 1×10^{-4} mol L^{-1} phenformin solution (pH 7.0) before and after adding 5×10^{-3} mol L^{-1} of various substances such as ascorbic acid, L-cysteine, D-fructose, D-glucose and L-phenylananine (Fig. 8B). It can be seen that all these substances

Table 1
Comparison for determination of phenformin by different methods.

Method	Linear range (μg mL^{-1})	LOD (μg mL^{-1})	Reference
Capillary electrophoresis	1–15	–	[28]
HPLC	5–100	0.065	[29]
Spectrophotometry	0.20–400	0.13	[30]
Chemiluminescence	0.09–2.0	0.031	[31]
Electrochemical biosensor	0.242–242	0.081	This work

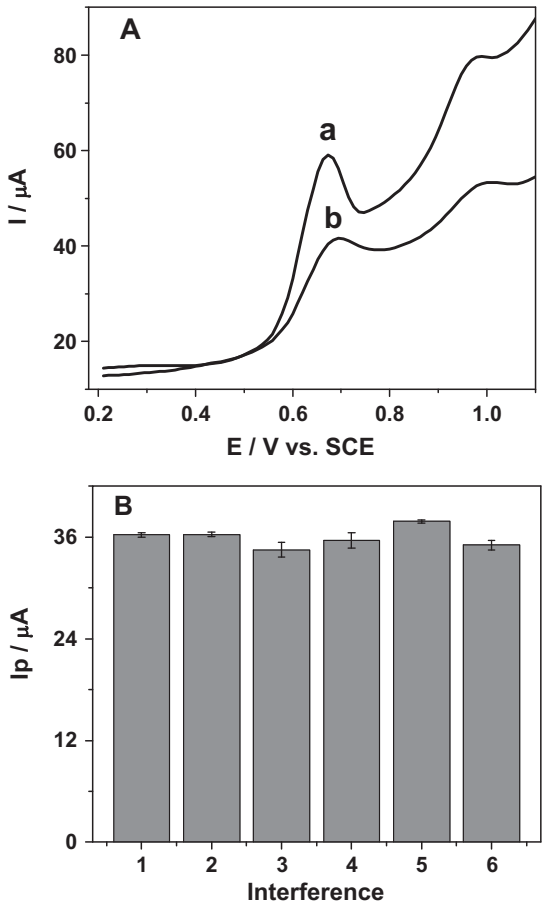

Fig. 8. (A) DPVs of DNA/GR-CdS/GCE in PBS (pH 7.0) without (a) and with (b) 1×10^{-3} mol L^{-1} phenformin. Interaction time: 100 s. DNA concentration: 0.7 mg mL^{-1}. (B) DPV peak currents of biosensor for 1×10^{-4} mol L^{-1} phenformin in PBS (pH 7.0) before (1) and after adding 5×10^{-3} mol L^{-1}, (2) ascorbic acid, (3) L-cysteine, (4) D-fructose, (5) D-glucose, and (6) L-phenylananine. Error bars were derived from the standard deviation of four measurements.

do not show noticeable interference in the determination of phenformin.

3.4.2. Application of biosensor to real sample analysis

The DNA/GR-CdS/GCE-based biosensor was utilized to determine the content of phenformin in a commercial medicine tablet. The tablet was accurately weighed, dissolved in water, filtered through a quantitative filter paper and then used as the medicine sample solution. After diluted with PBS (pH 7.0), the medicine sample solution was analyzed by DPV on DNA/GR-CdS/GCE under the aforementioned optimum conditions. The result showed that the content of phenformin in this medicine tablet was 26.09 mg per tablet. For comparison, the content of phenformin in the sample was also determined by HPLC after the sample solution was diluted with water. The HPLC result showed that the content of phenformin in the sample was 26.38 mg per tablet, which was close to the value obtained by DPV (Table 2).

Moreover, the proposed electrochemical biosensor was applied to the determination of phenformin in urine sample using the standard addition method. The fresh urine sample provided by a healthy female volunteer was used as the blank. After centrifugation, the upper layer of urine sample was collected and spiked with a known amount of phenformin standard solution. Then, the sample were diluted with PBS (pH 7.0) and analyzed by DPV using the proposed biosensor. At the same time, the samples were diluted with water and analyzed by HPLC. Table 3 compares the results

Table 2
Assay of phenformin in medicine tablet by the proposed DPV method compared with HPLC analysis ($n = 3$).

Sample	Found by proposed biosensor method (mg ± SD)	Found by HPLC method (mg ± SD)	Relative difference (%)
Phenformin tablet	26.09 ± 0.226	26.38 ± 0.432	1.10

Table 3
Analytical results of phenformin in spiked urine samples by the proposed DPV method compared with HPLC analysis ($n = 3$).

Sample no.	Concentration of phenformin			Recovery (%)	
	Added (10^{-5} mol L^{-1})	Found by proposed biosensor method (10^{-5} mol L^{-1} ± SD)	Found by HPLC (10^{-5} mol L^{-1} ± SD)	DPV	HPLC
1	1.0	0.9298 ± 0.154	0.9292 ± 0.254	92.98	92.92
2	4.0	3.729 ± 0.135	3.808 ± 0. 601	93.22	95.20
3	7.0	6.613 ± 0.885	6.388 ± 0.428	94.47	91.26

of DPV and HPLC analysis. It can be seen that the DPV analysis shows satisfactory recoveries for the determination of phenformin spiked in urine samples. Moreover, the DPV analytical results are consistent with the HPLC analytical results. This demonstrates the applicability of the proposed electrochemical biosensor based on DNA/GR-CdS/GCE for the determination of phenformin in biofluid samples.

4. Conclusions

We have developed a new approach for low temperature synthesis of GR-CdS nanocomposite. The as-prepared GR-CdS was found to dramatically promote the electrochemical response of DNA, which was superior to GO, GR or CdS. Based on DNA-immobilized GR-CdS electrode, a novel electrochemical biosensor for the determination of phenformin was developed. The proposed biosensor was successfully applied to the determination of phenformin in real samples, demonstrating the useful performance of GR-CdS nanocomposite for constructing electrochemical biosensors.

Acknowledgements

This work was supported by the National Natural Science Foundation of China (Grant No. 61172005), the National High Technology Research and Development Program of China (863 Program) (Grant No. 2012AA06A304), the Opening Foundation of State Key Laboratory of Chemo/Biosensing and Chemometrics (Grant No. 200908) and the Fundamental Research Funds for the Central Universities (Grant No. 2011TS062). The authors thank the Analytical and Testing Center of HUST for the help in the characterization of synthesized materials.

References

[1] H. Cai, N. Zhu, Y. Jiang, P. He, Y. Fang, Biosens. Bioelectron. 18 (2003) 1311.
[2] J. Wang, O. Rincón, R. Polsky, Electrochem. Commun. 5 (2003) 83.
[3] X. Liu, X. Qu, H. Fan, S. Ai, R. Han, Electrochim. Acta 55 (2010) 6491.
[4] F.C. Abreu, M.O.F. Goulart, A.M.O. Brett, Biosens. Bioelectron. 17 (2002) 913.
[5] J. Liu, C. Roussel, G. Lagger, P. Tacchini, Anal. Chem. 77 (2005) 7687.
[6] L. Hlavata, K. Benikova, V. Vyskocil, J. Labuda, Electrochim. Acta 71 (2012) 134.
[7] P. Kara, K. Kerman, D. Ozkan, B. Meric, A. Erdem, Z. Ozkan, M. Ozsoz, Electrochem. Commun. 4 (2002) 705.
[8] Q. Liu, J. Li, W. Tao, Y. Zhu, S. Yao, Bioelectrochemistry 70 (2007) 301.
[9] L. Wang, Y. Wang, J. Chen, L. Guo, Toxicology 262 (2009) 250.
[10] S. Chen, S. Chen, Electrochim. Acta 48 (2003) 4049.
[11] A.M. Tencaliec, S. Laschi, V. Magearu, M. Mascini, Talanta 69 (2006) 365.
[12] N. Prabhakar, K. Arora, S.P. Singh, H. Singh, Anal. Biochem. 366 (2007) 71.
[13] L. Wu, X. Lu, J. Jin, H. Zhang, J. Chen, Biosens. Bioelectron. 26 (2011) 4040.
[14] K. Kerman, Y. Morita, Y. Takamura, M. Ozsoz, E. Tamiya, Anal. Chim. Acta 510 (2004) 169.
[15] P. Arias, N.F. Ferreyra, G.A. Rivas, J. Electroanal. Chem. 634 (2009) 123.
[16] Y. Bo, H. Yang, Y. Hu, T. Yao, S. Huang, Electrochim. Acta 56 (2011) 2676.
[17] Z. Wang, J. Zhang, P. Chen, X. Zhou, Y. Yang, S. Wu, L. Niu, Y. Han, L. Wang, P. Chen, F. Boey, Q. Zhang, B. Liedberg, Biosens. Bioelectron. 26 (2011) 3881.
[18] W. Zhang, T. Yang, C. Yin, G. Li, Electrochem. Commun. 11 (2009) 783.
[19] I. Balan, I.G. David, V. David, A.I. Stoica, C. Mihailciuc, I. Stamatin, A.A. Ciucu, J. Electroanal. Chem. 654 (2011) 8.
[20] A. Cao, Z. Liu, S. Chu, M. Wu, Z. Ye, Z. Cai, Y. Chang, S. Wang, Q. Gong, Y. Liu, Adv. Mater. 22 (2010) 103.
[21] Q. Li, B. Guo, J. Yu, J. Ran, B. Zhang, H. Yan, J. Gong, J. Am. Chem. Soc. 133 (2011) 10878.
[22] M. Yang, A. Javadi, S. Gong, Sens. Actuators B 155 (2011) 357.
[23] K. Wang, Q. Liu, X. Wu, Q. Guan, H. Li, Talanta 82 (2010) 372.
[24] J. Lee, S.L. Chan, C. Lu, M.A. Lane, Exp. Neurol. 175 (2002) 161.
[25] F. Caraci, M. Chisari, G. Frasca, S. Chiechio, S. Salomone, A. Pinto, M.A. Sortino, A. Bianchi, Life Sci. 74 (2003) 643.
[26] Q. Aziz, A. Thomas, T. Khambra, A. Tinker, Eur. J. Pharmacol. 634 (2010) 26.
[27] M.I. Ortiz, Pharmacol. Biochem. Behav. 99 (2011) 1.
[28] E.P.C. Lai, S.Y. Feng, J. Chromatogr. B 843 (2006) 94.
[29] M. Lin, J. Lin, K. Wen, J. Food Drug Anal. 9 (2001) 139.
[30] M. Wang, Y. Zhang, Q. Li, J. Chin. Chem. Soc. 55 (2008) 1351.
[31] Z. Liu, F. Jia, W. Wang, C. Wang, Y. Liu, Luminescence 27 (2012) 297.
[32] L. Wei, J. Borowiec, L. Zhu, J. Zhang, Microchim. Acta 173 (2010) 439.
[33] A. Ferancová, S. Rengaraj, Y. Kim, J. Labuda, M. Sillanpää, Biosens. Bioelectron. 26 (2010) 314.
[34] C. Zhu, S. Guo, Y. Fang, S. Dong, ACS Nano 4 (2010) 2429.
[35] X. Yang, H. Ding, D. Zhang, X. Yan, C. Lu, J. Qin, R. Zhang, H. Tang, H. Song, Cryst. Res. Technol. 46 (2011) 1195.
[36] C. Unni, D. Philip, K.G. Gopchandran, Spectrochim. Acta A 71 (2008) 1402.
[37] S. Stankovich, R.D. Piner, S.T. Nguyen, R.S. Ruoff, Carbon 44 (2006) 3342.
[38] X. Zhao, S. Zhou, L. Jiang, W. Hou, Q. Shen, Chem. Eur. J. 18 (2012) 4974.
[39] A.G. Young, D.P. Green, A.J. McQuillan, Langmuir 22 (2006) 11106.
[40] E. Katz, I. Willner, Electroanalysis 15 (2003) 913.
[41] S. Liu, J. Liu, X. Han, Y. Cui, W. Wang, Biosens. Bioelectron. 25 (2010) 1640.
[42] Z. Xu, Y. Bando, L. Liu, W. Wang, X. Bai, D. Golberg, ACS Nano 5 (2011) 4401.
[43] E. Palecek, M. Bartosik, Chem. Rev. 112 (2012) 3427.
[44] L.M. Goncalves, C. Batchelor-McAuley, A.A. Barros, R.G. Compton, J. Phys. Chem. C 114 (2010) 14213.
[45] Q. Li, C. Batchelor-McAuley, R.G. Compton, J. Phys. Chem. B 114 (2010) 7423.
[46] K. Saeki, T. Kunito, M. Sakai, Biol. Fertil. Soils 46 (2010) 531.
[47] M.I. Pividori, A. Merkoci, S. Alegret, Biosens. Bioelectron. 15 (2000) 291.
[48] A.M.O. Brett, A.M. Chiorcea, Electrochem. Commun. 5 (2003) 178.